THE JOURNAL OF PHYSICAL CHEMISTRY LETTERS
A JOURNAL OF THE AMERICAN CHEMICAL SOCIETY

pubs.acs.org/JPCL Letter

Hydrogen Coupling on Platinum Using Artificial Neural Network Potentials and DFT

Peter S. Rice, Zhi-Pan Liu, and P. Hu*

Cite This: J. Phys. Chem. Lett. 2021, 12, 10637−10645 Read Online

ACCESS | Metrics & More | Article Recommendations | Supporting Information

ABSTRACT: To date, the understanding of reactions at solid−liquid interfaces has proven challenging, mainly because of the inaccessible nature of such systems to current experimental techniques with atomic resolution. This has meant that many important features, including free energy barriers and the atomistic structure of intermediates, remain unknown. To tackle these issues, we construct and utilize a high-dimensional neural network (HDNN) potential for the simulation of hydrogen evolution at the HCl(aq)/Pt(111) interface, taking into consideration the influence of adsorbate−adsorbate, adsorbate−solvent interactions, and ion solvation explicitly. Long time scale MD simulations reveal coadsorbed H_{ad}/H_2O_{ad} on the surface. The free energy profiles for the Tafel and Heyrovsky type hydrogen coupling are extracted using umbrella sampling. It is found that the preferential mechanism can change depending on the surface coverage, highlighting the dual mechanistic nature for HER on Pt(111). Our work demonstrates the importance of controlling the solvent−substrate interactions in developing catalysts beyond Pt.

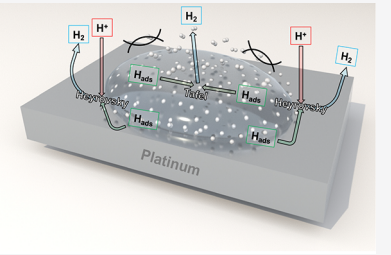

Downloaded via FUDAN UNIV on October 28, 2021 at 00:36:55 (UTC).
See https://pubs.acs.org/sharingguidelines for options on how to legitimately share published articles.

With increasing energy demands, emphasis has been placed on carbon-neutral technologies as alternatives to fossil fuels because of their reduced environmental footprint and to mitigate greenhouse gas emissions into the atmosphere.[1,2] One potential candidate is molecular hydrogen (H_2), which has been known for decades to be the cleanest possible energy carrier, boasting zero carbon dioxide emissions and possessing the largest energy density of known combustible fuels.[3−5] The most attractive route for H_2 production is the electrocatalytic splitting of water ($H_2O \rightleftharpoons H_2 + \frac{1}{2}O_2$)[6,7] in electrical cells, amounting to two individual half-cell reactions. The most extensively examined reaction is the hydrogen evolution reaction (HER), which occurs at the cathode.[8] Under acidic conditions HER proceeds *via* two possible mechanisms, and each is composed of an adsorption and desorption elementary step:[9,10]

$$H_3O^+ + e^- \rightleftharpoons H_{ads} + H_2O \quad \text{(Volmer)} \tag{1}$$

$$H_{ads} + H_{ads} \rightleftharpoons H_2 \quad \text{(Tafel)} \tag{2}$$

$$H_{ads} + H_3O^+ + e^- \rightleftharpoons H_2O + H_2 \quad \text{(Heyrovsky)} \tag{3}$$

The first is the combination of eqs 1 and 2, which is known as the Volmer−Tafel mechanism, whereby an initial proton adsorption from the solution onto the surface is followed by surface coupling and subsequent desorption of molecular hydrogen. The second mechanism differs only in the process of desorption; the surface coupling is replaced with a charge-transfer step, eq 3; the overall process is known as the Volmer−Heyrovsky mechanism. It is worth noting that HER is also a central reaction in the photocatalytic splitting of water,[11−16] in which adsorbed metal nanoparticles (*e.g.*, Pt, Pd, and Ni) act as cocatalysts on support surfaces. It is clear that understanding the H_2 coupling step is of critical interest for catalyst design.

Despite significant efforts to move away from platinum (Pt), the outlook of HER on Pt remains the most promising, because of its exceptional catalytic activity compared with that of other transition metals and materials.[17] However, while a great deal is known regarding HER on Pt, experimental investigations reveal a chemically complex solid−liquid reaction environment.[18−23] For instance, from Tafel slope measurements a clear mechanistic preference for HER is found on Pt(110) and Pt(100) surfaces, while the mechanism on Pt(111), the most stable Pt surface, is still being debated in the literature.[24−31] There is a good reason for the slow progress in understanding HER. Experimentally, the low resolutions obtained from spectroscopic analyses are inadequate for analyzing the complicated solid−liquid interfacial structure; the exact nature of weakly bound adsorbates on (111) surfaces cannot be directly identified using current experimental methods because of high surface mobilities and diffusion rates.[32] To this end, theoretical modeling of solid−liquid interfaces has been extensively used.[33−37] Notable progress has been made, showcasing the inherent value of *ab initio*

Received: September 12, 2021
Accepted: October 25, 2021

ACS Publications © XXXX American Chemical Society

https://doi.org/10.1021/acs.jpclett.1c02998
J. Phys. Chem. Lett. 2021, 12, 10637−10645

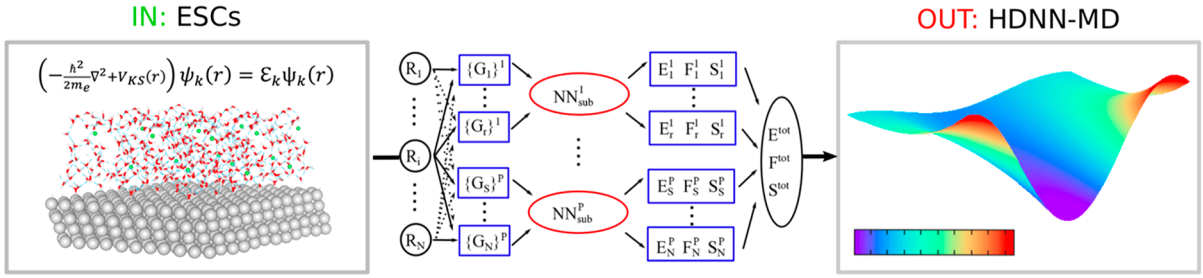

Figure 1. Schematic representation of how the high-dimensional neural network potential is generated. Electronic structure calculations (ESCs) are used as the initial inputs (IN) before being fed through the artificial neural network architecture, outputting (OUT) a high-dimensional neural network potential (HDNN) for further molecular dynamics (MD) simulation.

molecular dynamics (AIMD) and related methods in understanding experimental findings.[38−48] However, several pitfalls emerge depending on the choice of method, while extracting free energy profiles at the solid−liquid interface with explicit solvent remains a formidable task. Additionally, more open challenges remain, such as determining the extent to which the solvent environment and surface adsorbed hydrogen species influence the reactivity. Of particular importance is deciphering the effects of interactions at the interface such as ion solvation, solvent−surface, solvent−adsorbate and adsorbate−adsorbate.

In this work, we aim to tackle several of these aforementioned questions using a combined machine learning and DFT approach to model the H_2O/Pt(111) interface in the presence of solvated chlorine (Cl) ions, giving a quantitative interpretation of the structure and associated reactivity based on long time scale MD simulations. This is achieved by adopting a carefully optimized high-dimensional neural network (HDNN) potential along with first-principles *ab initio* calculations. Using DFT calculations, we find that a balance between solvent−adsorbate and adsorbate−adsorbate interactions dictates the adsorption site and the reactivity. Finally, the energetic barriers for hydrogen coupling are examined using the stochastic surface walk reaction sampling (SSW-RS) method and umbrella sampling (US). Whereby, we arrive at a coherent mechanistic explanation for HER on Pt(111) which is dictated by coadsorbed H_{ad}/H_2O_{ad}.

Methodology. Simulating solid−liquid interfaces using AIMD allows for an accurate description of the electronic structure and chemical interactions between the surface and solvent molecules. However, AIMD is hindered by the prohibitively long time scales and large system sizes often required to equilibrate the solvent dynamics. To circumvent this, machine learning (ML) and other artificial intelligence (AI) methodologies have been recognized as an immediate front runner. In particular, artificial neural network (NN) training techniques have demonstrated great promise in generating potentials that have several distinct advantages over AIMD and traditional *ab initio* electronic structure calculation (ESC) methods.[49−52] First, fitting the potential energy surface (PES) generated from high-level ESCs for the prediction of bond breaking/making mechanisms[53−55] has shown promise for reaction pathway sampling of complex catalytic systems.[56,57] Second, NNs exhibit a distinct mark-up in computation speed due to the scaling no longer being dependent on the number of electrons, compared with DFT calculations.[58] When properly trained, the generated potential can predict the system energy within a close range of DFT accuracy, coupled with MD time scales typically reserved for classical force field simulation.[59−63] These features of NN-trained potentials make them an effective tool for investigating solid−liquid interfaces. The general process of generating the HDNN potential is schematically summarized in Figure 1.

Specifically, in this work we use the high-dimensional neural network molecular dynamics simulation (HDNN-MD) carried out using the Large-scale Atomic Simulation with neural network Potential (LASP) code.[64] To develop a well-converged potential for the prediction of reaction energetics at the solid−liquid interface, it is necessary to obtain an initial training set that can cope with the numerous configurations associated with the complexities of the liquid ad-layers. Here, the initial data training set is obtained using the stochastic surface walking (SSW) global optimization method[65] based on DFT schemes, which by design, fully explores the PES.[66] The high-dimensional NN (HDNN) potential is itself generated using a modification of the pioneering Behler−Parrinello method,[67] where the input layer utilizes a unique set of power-type structure descriptors (PTSD) developed by Liu and co-workers[68] (eqs S4−S9). Here, the total energy (E_{total}) is expressed as the sum of the individual atomic contributions (E_i), eq 4:

$$E_{\text{total}} = \sum_i E_{i,p} \tag{4}$$

The energy of each atom i of element type p is calculated, which can be output from the standard NN for this element.

The applicability of our HDNN potential is tested to ensure consistency with the PES generated from ESCs, thus allowing for simulations of much larger systems, with the additional benefit of predicting energies of previously unknown configurations. Once generated, it becomes possible to modify the atomic interactions to correct for environment-dependent van der Waals (vdWs) interactions, such as the Grimme's D3 correction.[69] VdWs are critically important when simulating water, having recently been shown to be of fundamental importance in describing key properties, such as the anomalous density of liquid water compared to ice under ambient conditions[70−72] and for an accurate description of the cohesive properties of species on metal surfaces.[73]

Our NN potential has been extensively tested to assess its applicability for characterizing the structure of water on a p(4 × 4) layer Pt(111) slab, consisting of 44 H_2O molecules with two solvated Cl atoms, shown in Figure S1. A 202-atom unit cell permits validation with DFT at several levels of theory. However, it should be noted that the transferability of the generated NN potential to system sizes several orders of magnitude larger exists. The final Pt−O−H−Cl training data set consists of 77 120 structures; the root-mean-square (RMS) errors for the energy and the force of the HDNN potential are

https://doi.org/10.1021/acs.jpclett.1c02998
J. Phys. Chem. Lett. 2021, 12, 10637−10645

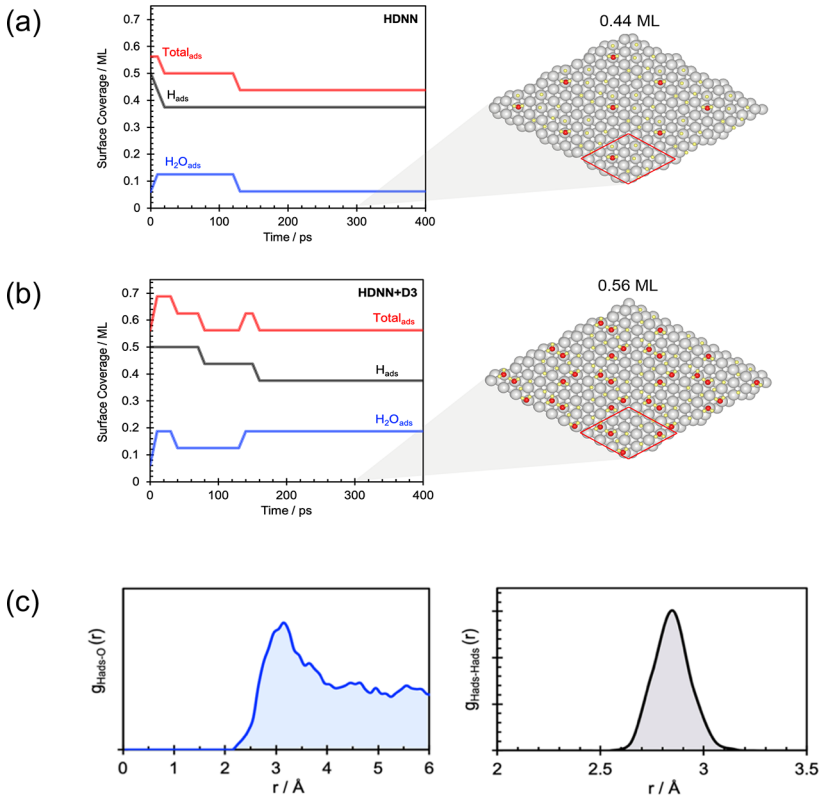

Figure 2. (a) Surface coverage of H_{ads} and H_2O_{ads} from a 400 ps high-dimensional neural network potential molecular dynamics (HDNN-MD) simulations. (b) Surface coverage with additional D3 correction to HDNN. Snapshots after 300 ps are shown on the right along with the total coverage. (c) AIMD calculated $g(r)$ highlighting the adsorbate−adsorbate and adsorbate−solvent separation distance.

2.964 meV/atom and 0.072 eV/Å, respectively. The final Pt−O−H−Cl potential and training data set is openly accessible from the LASP Web site (www.lasphub.com). More details regarding the generation and testing of the HDNN potential are provided in the Supporting Information along with details on the stochastic surface walk reaction sampling (SSW-RS) method. Unless otherwise stated, we have confirmed all energy minima and pathways by umbrella sampling coupled with DFT calculations.

Examination of Adsorbate−Adsorbate and Adsorbate−Solvent Interactions. To assess the stability of hydrogen on the Pt(111) surface, we begin by covering all fcc-hollow site positions with adsorbed hydrogen (H_{ads}) and run a 400 ps HDNN-MD simulation with and without D3 vdW correction, as shown in Figure 2a,b. Configurations from the last 100 ps of our HDNN-MD simulations were further equilibrated and validated using 5 ps AIMD simulations at the PBE-D3 level of theory. Three striking features can be found from our simulations. First, a steady-state coverage occurs after ∼300 ps within the canonical ensemble, resulting in a surface coverage of 0.44 ML for the uncorrected HDNN potential and 0.56 ML with D3 vdW correction. This result is in good agreement with experimental results by Marković et al.[25] who reported a partial coverage of ∼0.66 ML. Second, in addition to H_{ads}, there exist some water molecules coadsorbed on the surface. More specifically, for water to adsorb, hydrogen must first be displaced from the surface, where water can interact with bare Pt(111) top sites. Adsorbed water has been found to be of critical importance in describing the negative capacitive response of Pt(111) in aqueous solvent.[74] Third and perhaps more importantly, H_{ads} and H_2O_{ads} form patches on the surface resulting in regions of high and low H_{ads} coverages (Figure 2a,b).

Careful examination of H_{ads}/H_2O_{ads} patches shows that the adsorption of H_2O is strictly localized on the Pt(111) top site *via* the $1b_1$ molecular orbital and the Pt d-band.[75,76] This observation is supported by classical MD simulations by Limmer et al.[77] on the pure water−Pt(111) interface. However, on a hydrogen-covered surface, water adsorption is found to occur rarely throughout the simulation time frame (∼20−100 ps) and proceeds only with displacement of neighboring hydrogen atoms by H_2O_{ads}. Considering that hydrogen and water have a comparable binding energy[78,79] on Pt(111), it could be the combination of both species that contributes to the observed experimental surface coverage. Furthermore, the displacement of H_{ads} by H_2O_{ads} may be expected to be a unique feature of the (111) crystallographic interface. Chandler and co-workers[80] carried out classical MD simulations and suggested that the 6-fold coordination on Pt(111) creates additional interfacial disorder and can facilitate molecule exchange. Additionally, Kronberg and Laasonen[47] exemplified, *via* extensive AIMD calculations, how this type of H/H_2O molecular exchange can result in solvent fluctuations and a modulation of the interfacial electrostatics.

To understand the above results, the interfacial region is analyzed and several key structural descriptors, such as radial pair distribution functions ($g(r)$), have been calculated at several levels of theory. On calculating $g(r)$ to characterize $H_{ads}−H_{ads}$ and $H_{ads}−H_2O$ separation density, it is found that the adsorbed hydrogen species interacts repulsively with neighboring solvent and coadsorbed hydrogen on the surface of ∼2.9 Å (Figure 2c). The separation distance for $H_{ads}−H_{ads}$

https://doi.org/10.1021/acs.jpclett.1c02998
J. Phys. Chem. Lett. 2021, 12, 10637−10645

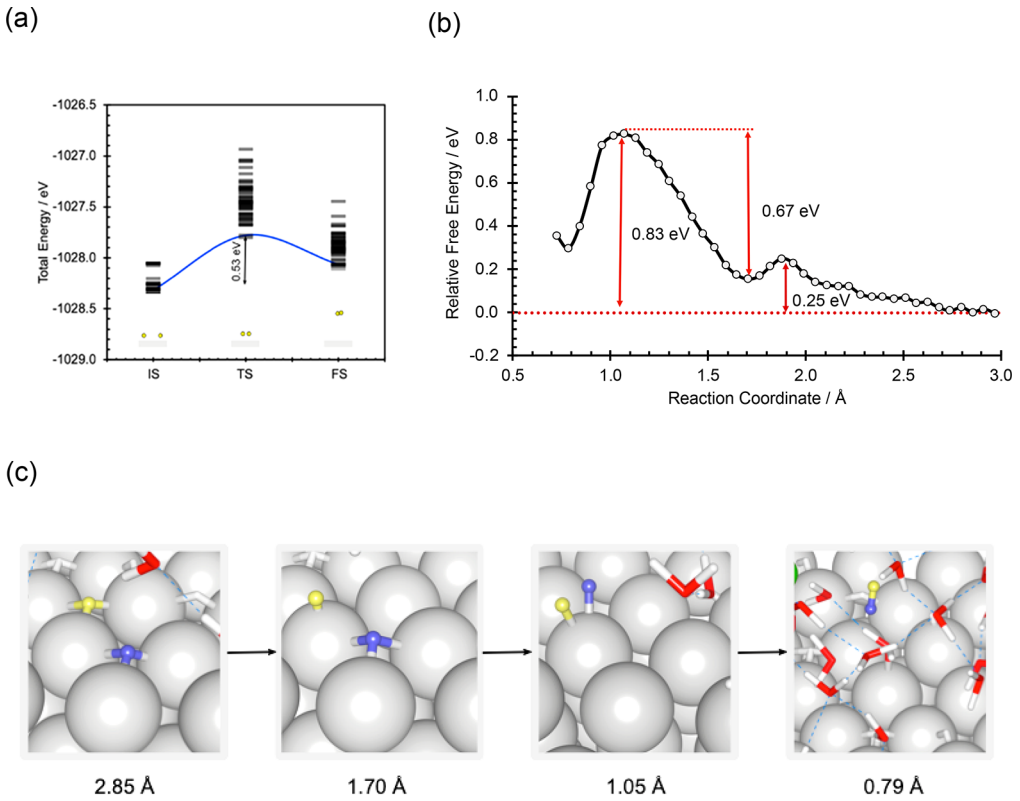

Figure 3. (a) Calculated total energy states for the Tafel reaction, highlighting the energy change between the initial (IS), transition (TS) and final states (FS) using the stochastic surface walk reaction sampling methodology (SSW-RS) within the HDNN+D3 level of theory. (b) Free energy profile for surface coupling of adsorbed hydrogen species (Tafel mechanism) calculated using umbrella sampling with HDNN+D3. (c) Snapshots of our proposed pathway for hydrogen coupling on the surface, extracted from the HDNN simulation trajectories. (The hydrogen species are shown in blue and yellow, while additional solvent species have been removed for clarity.)

and H_{ads}−H_2O can be attributed to the balance of interaction between the frontier molecular orbitals of water ($(2a_1)^2(1b_2)^2(3a_1)^2(1b_1)^2$), adsorbed hydrogen and the Pt(111) d-electrons. This observation is consistent with findings from our recent paper[81] on the topic; a dipole repulsion effect of a single hydrogen species with the surrounding water molecules (maintained at ∼2.95 Å) is found to be critical in describing the adsorption behavior of hydrogen on Pt(111) *via* diffusion from the top site to the hollow site.

This is an important issue to consider because it is of fundamental importance for the mechanism of H_2 formation on Pt. The effect itself is attributed to the Pauli type repulsion exhibited by the accumulation of a small negative charge in the vicinity of the H_{ads} species and the lone pair belonging to the water. Furthermore, this repulsion also exists between neighboring H_{ads} which, interestingly, is maintained at the same repulsive radius. At greater surface coverage, it is the balance of these repulsive forces at the Pt(111) interface that allows for the fcc-hollow sites to be occupied by H_{ads} in the presence of liquid water. The aforementioned accumulation of H_{ads} with the repulsive sphere ensures a stable area of hydrogen which is maintained by the accumulation of H_{ads}. Only hydrogen species close to the edge of such domains can readily desorb into the solution where H_2O can come within close proximity to displace such species. Recently, Sakong and Groß[82] performed AIMD simulations, in which they modeled a 1 ML hydrogen coverage for 40 ps, and observed that water is repelled by an additional 1.0 Å from the Pt(111) surface. Their work is consistent with our results.

Next, to assess the influence of solvated ions on the structure and dynamics of the solvent layer, we calculated the first solvation shell around Cl, as $n^{Cl}_{O/H} = \int_0^{r_N} 4\pi r^2 \varrho g_{Cl-O/H}(r)\, dr$, where ϱ is the periodicity constant and $g_{Cl-O/H}(r)$ is the radial distribution function for Cl−O/H with the first minimum at r_N (see Figure S3c). The resulting values of $n^{Cl}_O = 5.2$ and $n^{Cl}_H = 5.5$ are indicative of an ion-induced perturbation of the tetrahedrality of neighboring water molecules ($n^O_O \approx 4.0-5.0$ for pure water). This finding is in agreement with recent photoelectron spectroscopy and theoretical study by Pohl et al.[83] who found that solvated sodium (Na^+) and iodide (I^-) have little effect on the electronic structure of water, while ion-induced perturbations of the ideal tetrahedral configuration of water molecules were observed.

Furthermore, by measuring the bond and structural relaxation lifetimes we can assess the extent to which hydrogen bond dynamics is influenced by solvated Cl[84] (see the Supporting Information for details). The overall dynamics of the hydrogen-bond structural relaxation is found to be an order of magnitude slower than that of hydrogen-bond breaking, occurring in the subpicosecond time scale, because of a reduction of the effective strength of hydrogen bonds in the presence of solvated chloride ions. The hydrogen-bond structural relaxation occurs at a longer time scale (10.2 ps) because of additional interaction of water molecules with chloride ions resulting in a lengthening of the reorientational diffusion of water molecules ($D_0 \approx 1.64 \times 10^{-9}$ m^2/s). This observed strengthening of the hydrogen bond relaxation time, coupled with the pseudo-octahedral arrangement of water molecules surrounding Cl, suggests that solvated ions act to

https://doi.org/10.1021/acs.jpclett.1c02998
J. Phys. Chem. Lett. 2021, 12, 10637−10645

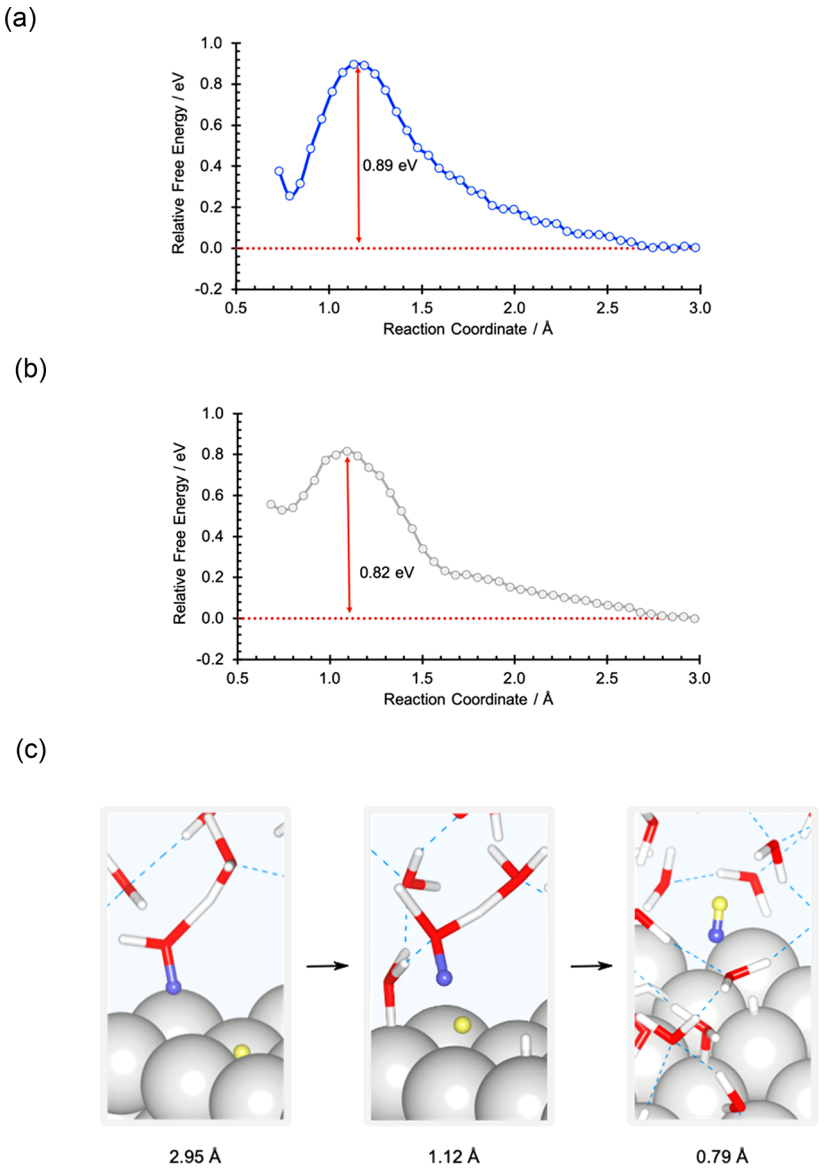

Figure 4. Free energy profiles for the coupling of an adsorbed hydrogen and a solvated hydrogen species (Heyrovsky mechanism) calculated using umbrella sampling with HDNN+D3 with (a) a high coverage of 0.56 ML and (b) a lower coverage of 0.33 ML (c) Snapshots of the proposed pathway for hydrogen coupling on the surface, extracted from the HDNN simulation trajectories.

distort the tetrahedrality of the water network resulting in weaker water−water interactions which could facilitate hydrogen transfer to the Pt(111) surface.

Tafel Mechanism Free Energy Profile. In an effort to determine the lowest-energy pathway for hydrogen coupling, we calculated both the total energy profile using the SSW-RS method and the free energy profile with umbrella sampling (US). The main objective of the SSW-RS method is to obtain a minimum-energy reaction trajectory, highlighted in Figure 3a (see also Figure S5). The SSW method[85] generates a number of reaction microstates in the form of reactant and product pairs (R/P), while the double-ended surface walk (DESW) method[86] is employed to locate the transition state for all generated R/P pairs. This ensures the configuration for the lowest-energy reaction barrier to be calculated.

To further analyze our trajectory and to assess the influence of solvent dynamics, we used the generated HDNN potential coupled with the US method, and the free energy profiles for hydrogen adsorption/desorption are obtained and summarized in Figure 3b,c. Starting from two H_{ads} at neighboring fcc-hollow sites, we applied harmonic constraints to acquire the population along the H_{ads}−H_{ads} collective variable, driving H to couple along a series of simulation windows. Figure 3b represents the lowest-energy pathway for H desorption from the Pt(111) surface to the aqueous solution. Snapshots from the sampled trajectories are shown in Figure 3c, which have been selected under the guidance of calculated free energy values. It should be noted that the structural nature of the transition state species for both AIMD and HDNN are virtually indistinguishable.

From our simulations of the free energy profile, we can see that the reaction proceeds as follows: The initial state (IS) is at 2.85 Å between the hydrogen atoms, where the hydrogen species occupy neighboring fcc-hollow sites. A small diffusion barrier of 0.25 eV must be overcome from the IS to an intermediate state (IMS) located at the H−H distance of 1.70 Å, where one species experiences both adsorbate−adsorbate interaction and adsorbate−solvent interactions by relocating to

https://doi.org/10.1021/acs.jpclett.1c02998
J. Phys. Chem. Lett. 2021, 12, 10637−10645

the top site position, while the other H_{ads} remains on the fcc-hollow site. Finally, the most energetically demanding process is when both H_{ads} atoms come into close proximity for H_2 formation, where the fcc-hollow site species diffuses to the same top site position. This process proceeds with a barrier of 0.67 eV to overcome the transition state (TS) located at an H−H separation distance of 1.05 Å. Our calculated barrier is in excellent agreement with recent constrained-AIMD calculations by Kronberg and Laasonen,[48] in which the barrier for the Tafel mechanism exhibits a coverage dependence, decreasing from 0.80 eV (0.66 ML) to 0.53 eV (1.00 ML). To validate the reliability of our calculated free energy, we compare the HDNN with AIMD simulations, resulting in a mean averaged error (MAE) of ∼0.1 eV between the two calculation methods, as shown in Figure S6 and Table S2 (Supporting Information).

Heyrovsky Mechanism Free Energy Profile. To determine which mechanism is favored for HER on Pt(111) at PZC, the Heyrovsky mechanism ($H_{ads} + H_3O^+ + e^- \rightleftharpoons H_2 + H_2O$) should be analyzed in terms of free energy. The free energy profiles are obtained using the US approach, and the results are shown in Figure 4a−c. Here, one H_{ads} is located in the fcc-hollow site while the other is solvated in solution, and harmonic constraints are applied to acquire the population along the H_{ads}−H_3O^+ collective variable. Snapshots from the sampled trajectories are shown in Figure 4c. Similarly to the Tafel mechanism, the reliability of the calculated HDNN free energy is compared with AIMD simulations, shown in Figure S7 and Table S3 (Supporting Information).

From these simulations, it is found that the reaction proceeds without an initial diffusion barrier: At the IS, the distance between a hydrogen species in the fcc-hollow site and in the solvated Zundel cation ($H_5O_2^+$) is 2.95 Å. The reaction process proceeds with a barrier of 0.89 eV to overcome the TS located at 1.12 Å, whereby the H_{ads} species couples with the solvated proton above the Pt top site. Our calculated barriers are in agreement with theoretical studies by Liu and co-workers[87] (0.92 eV) using static DFT calculations coupled with a continuum solvation model and Yang et al.[88] (∼0.77 eV) who used constrained AIMD at the aqueous Pt(111) interface. Interestingly, the barrier can be reduced to 0.82 eV under conditions of low H_{ads} coverage or edge sites (shown in Figure 4b,c). It is found that in areas with lower hydrogen coverage, a hydrated proton can come within a closer proximity to react with H_{ads}, suggesting that at high coverage a "blanket" of repulsion is exhibited toward neighboring solvent molecules, resulting in a more hydrophobic surface which disfavors Eley−Rideal type reaction mechanisms.

Implications for HER. From our calculated free energy profiles, we can see that the Volmer−Tafel mechanism is favored over the Volmer−Heyrovsky mechanism on Pt(111) at high H coverage. The Tafel mechanism proceeds with an initial diffusion barrier of 0.25 eV from the fcc-hollow site to the top site position, followed by a coupling barrier of 0.67 eV (the effective barrier is 0.83 eV), while the repulsive nature toward water species inhibits a proton reacting with adsorbed species, resulting in the Heyrovsky mechanism proceeding with a larger barrier of 0.89 eV. Interestingly, our calculated free energy barrier is in agreement with the experimentally measured activation energy (0.5−0.6 eV) by Schmickler and co-workers.[30] However, the barrier of the Heyrovsky mechanism can be reduced when lower-coverage domains are sampled. The inverse behavior is predicted for the Tafel mechanism barrier, which has been shown to increase at lower coverage.[48] This is significant, as it suggests the dual mechanistic nature for HER on Pt(111) which is highly coverage-dependent.

We suggest that the influence of combined hydrogen/water coverage at varying potential is critical in describing the rate-determining step for the HER on Pt(111). At the center of the hydrogen-rich areas, where the adsorbate−adsorbate repulsive interaction is at its greatest, hydrogen is seen to be stabilized. This is indicated by the narrow probability distribution of the H_{ads}−H_{ads} peaks shown in Figure 2c. The Tafel mechanism is favored under these conditions, as a solvated proton in solution is sterically disfavored from reacting with such species, allowing for top site positions to be available for hydrogen coupling. These free reaction centers at the top sites are dictated by the interaction between the solvent and adsorbates at the interface.

On conducting a potential sweep, the surface coverage has been shown to inherently change,[37] resulting in the rate-determining mechanism also changing because of decreased adsorbate−adsorbate and adsorbate−solvent interactions. Our analysis could give insight into the mechanistic efficiency of H_2 formation on Pt(111), whereby both mechanisms can occur simultaneously depending on the surface coverage, with the ideally situated top site positions remaining free for hydrogen coupling to occur. Our analysis is consistent with the observed indistinguishability of the Tafel ($H_{ads} + H_{ads} \rightleftharpoons H_2$) and Heyrovsky ($H_{ads} + H_3O^+ + e^- \rightleftharpoons H_2 + H_2O$) mechanism from experimental cyclic voltammetry studies.[25,29] It should be noted that despite our findings being of general importance for pristine metal surfaces, the transferability of our findings to stepped or defect-containing surfaces remains unknown.

In conclusion, we have performed extensive HDNN-MD sampling methodologies and DFT calculations to study the reaction efficiency of hydrogen coupling at the H_2O/Pt(111) interface and obtained an atomistic picture of how the aqueous medium effects the structure and reactivity of HER. Based on our calculations and analyses, the following conclusions can be drawn:

(1) The high-dimensional neural network (HDNN), coupled with Grimmes D3 vdWs corrections, provides an efficient way for calculating the free energy barriers for surface reactions. Long time scale molecular dynamics simulations are required before a steady state of adsorbed hydrogen is found at the interfacial region, giving rise to H_{ad}/H_2O_{ad} patches on the surface.

(2) The interaction of hydrogen atoms with their surroundings in the form of adsorbate−adsorbate and adsorbate−solvent interactions is critical in describing the preference for H_{ads} at the fcc-hollow site and the interactions of H_{ads} with its surrounding environment dictates the preferential reaction mechanism for H_2 formation.

(3) The energetics obtained from our calculations point to two distinct mechanisms for H_2 formation depending on the surface coverage: the Volmer−Tafel mechanism is preferred in areas of high coverage, while the repulsive forces dictate that the Heyrovsky mechanism is hindered and permitted only at low coverage. Thus, the simulations could give an explanation for the efficiency of HER on Pt(111) *via* the availability of both reaction pathways depending on the surface coverage.

https://doi.org/10.1021/acs.jpclett.1c02998
J. Phys. Chem. Lett. 2021, 12, 10637−10645

■ ASSOCIATED CONTENT

Supporting Information

The Supporting Information is available free of charge at https://pubs.acs.org/doi/10.1021/acs.jpclett.1c02998.

Computational methods, unit cell and energy convergence, structural tests, radial pair distribution function, stochastic surface walk−reaction sampling, high-dimensional neural network potential, and electrostatic correction (PDF)

■ AUTHOR INFORMATION

Corresponding Author

P. Hu − *School of Chemistry and Chemical Engineering, The Queen's University of Belfast, Belfast BT9 5AG, Northern Ireland;* orcid.org/0000-0002-6318-1051; Email: p.hu@qub.ac.uk

Authors

Peter S. Rice − *School of Chemistry and Chemical Engineering, The Queen's University of Belfast, Belfast BT9 5AG, Northern Ireland;* orcid.org/0000-0003-2946-3781

Zhi-Pan Liu − *Shanghai Key Laboratory of Molecular Catalysis and Innovative Materials, Department of Chemistry, Key Laboratory of Computational Physical Science (Ministry of Education), Fudan University, Shanghai 200433, China;* orcid.org/0000-0002-2906-5217

Complete contact information is available at: https://pubs.acs.org/10.1021/acs.jpclett.1c02998

Notes

The authors declare no competing financial interest.

■ ACKNOWLEDGMENTS

P.H. and P.S.R. acknowledge the use of computational resources at the UK national high-performance computing service, ARCHER, for which access was obtained *via* the UKCP consortium. We are grateful to the UK Materials and Molecular Modelling Hub for computational resources, which is partially funded by EPSRC (EP/P020194/1). P.S.R. acknwoledges his Ph.D. studentship funded by the Northern Ireland Department for the Economy (NI-DfE) at the Queen's University of Belfast.

■ REFERENCES

(1) Koroneos, C.; Spachos, T.; Moussiopoulos, N. Exergy analysis of renewable energy sources. *Renewable Energy* **2003**, *28*, 295−310.

(2) Shafiee, S.; Topal, E. When will fossil fuels be diminished? *Energy Policy* **2009**, *37*, 181−189.

(3) Veziroglu, T. N.; Barbir, F. Hydrogen: the wonder fuel. *Int. J. Hydrogen Energy* **1992**, *17* (6), 391−404.

(4) Verhelst, S. Recent progress in the use of hydrogen as a fuel for internal combustion engines. *Int. J. Hydrogen Energy* **2014**, *39* (2), 1071−1085.

(5) Rigden, J. S. *Hydrogen, the essential element*; Harvard University Press, 2002.

(6) Dubouis, N.; Grimaud, A. The hydrogen evolution reaction: from material to interfacial descriptors. *Chem. Sci.* **2019**, *10*, 9165−9181.

(7) de Levie, R. The electrolysis of water. *J. Electroanal. Chem.* **1999**, *476* (1), 92−93.

(8) Dresselhaus, M. S.; Thomas, I. L. Alternative energy technologies. *Nature* **2001**, *414*, 332−337.

(9) Bockris, J. O'M.; Conway, B. E. *Modern Aspects of Electrochemistry*; Butterworths Sci. Publications: England, 1954; Vol. *1* (Chapter 4).

(10) Conway, B. E.; Tilak, B. V.; Eley, D. D.; Pines, H.; Weisz, P. B. *Advances in Catalysis*; Academic Press Inc.: New York, 1992; Vol. *38* (Chapter 1).

(11) Wang, D.; Sheng, T.; Chen, J.; Wang, H.-F.; Hu, P. Identifying the key obstacles in photocatalytic oxygen evolution on rutile TiO_2. *Nat. Catal* **2018**, *1*, 291−299.

(12) Wei, G. F.; Liu, Z. P. Restructuring and hydrogen evolution on Pt nankoparticles. *Chem. Sci.* **2015**, *6*, 1485.

(13) Li, Y. F.; Liu, Z. P. Particle size, shape and activity for photocatalysis on titania anatase nanoparticles in aqueous surroundings. *J. Am. Chem. Soc.* **2011**, *133*, 15743.

(14) Wang, D.; Liu, Z. P.; Yang, W. M. Revealing the Size Effect of Platinum Cocatalyst for Photocatalytic Hydrogen Evolution on TiO_2 Support: A DFT Study. *ACS Catal.* **2018**, *8*, 7270.

(15) Wang, D.; Liu, Z. P.; Yang, W. M. Proton-promoted electron transfer in photocatalysis: key step for photocatalytic hydrogen evolution on metal/titania composites. *ACS Catal.* **2017**, *7*, 2744.

(16) Rice, P. S.; Hu, P. Understanding supported noble metal catalysts using first-principle calculations. *J. Chem. Phys.* **2019**, *151*, 180902.

(17) Kibsgaard, J.; Tsai, C.; Chan, K.; Benck, J. D.; Nørskov, J. K.; Abild-Pedersen, F.; Jaramillo, T. F. Designing an Improved Transition Metal Phosphide Catalyst for Hydrogen Evolution Using Experimental and Theoretical Trends. *Energy Environ. Sci.* **2015**, *8* (10), 3022−3029.

(18) Conway, B. E.; Salomon, M. Studies on the Hydrogen Evolution Reaction Down to—150 C and the Role of Proton Tunnelling. *J. Chem. Phys.* **1964**, *41*, 3169.

(19) Agmon, N. The grotthuss mechanism. *Chem. Phys. Lett.* **1995**, *244*, 456.

(20) Schmickler, W.; Santos, E. *Interfacial Electrochemistry*; Oxford Univ. Press: New York, 1996.

(21) van der Vliet, D.; Strmcnik, D. S.; Wang, C.; Stamenkovic, V. R.; Markovic, N. M.; Koper, M. T. M. On the importance of correcting for the uncompensated Ohmic resistance in model experiments of the Oxygen Reduction Reaction. *J. Electroanal. Chem.* **2010**, *647*, 29−34.

(22) Carrasco, J.; Hodgson, A.; Michaelides, A. A molecular perspective of water at metal interfaces. *Nat. Mater.* **2012**, *11*, 667−674.

(23) Peng, J.; Cao, D.; He, Z.; Guo, J.; Hapala, P.; Ma, R.; Cheng, B.; Chen, J.; Xie, W. J.; Li, X. Z.; Jelínek, P.; Xu, L. M.; Gao, Y. Q.; Wang, E. G.; Jiang, Y. The Effect of Hydration Number on the Interfacial Transport of Sodium Ions. *Nature* **2018**, *557* (7707), 701−705.

(24) Conway, B. E.; Barber, J.; Morin, S. Comparative evaluation of surface structure specificity of kinetics of UPD and OPD of H at single-crystal Pt electrodes. *Electrochim. Acta* **1998**, *44*, 1109.

(25) Marković, N. M.; Grgur, B. N.; Ross, P. N. Temperature-dependent hydrogen electrochemistry on platinum low-index single-crystal surfaces in acid solutions. *J. Phys. Chem. B* **1997**, *101*, 5405−5413.

(26) Conway, B. E.; Jerkiewicz, G. Relation of energies and coverages of underpotential and overpotential deposited H at Pt and other metals to the 'volcano curve' for cathodic H_2 evolution kinetics. *Electrochim. Acta* **2000**, *45*, 4075−4083.

(27) Tavares, M.; Machado, S. A.; Mazo, L. Study of hydrogen evolution reaction in acid medium on Pt microelectrodes. *Electrochim. Acta* **2001**, *46*, 4359−4369.

(28) Kunimatsu, K.; Senzaki, T.; Tsushima, M.; Osawa, M. A combined surface-enhanced infrared and electrochemical kinetics study of hydrogen adsorption and evolution on a Pt electrode. *Chem. Phys. Lett.* **2005**, *401*, 451−454.

(29) Watzele, S.; Fichtner, J.; Garlyyev, B.; Schwämmlein, J. N.; Bandarenka, A. S. On the Dominating Mechanism of the Hydrogen

Evolution Reaction at Polycrystalline Pt Electrodes in Acidic Media. *ACS Catal.* **2018**, *8*, 9456−9462.
(30) He, Z.-D.; Wei, Z.; Chen, Y.; Santos, E.; Schmickler, W. Hydrogen evolution at Pt(111) - activation energy, frequency factor and hydrogen repulsion. *Electrochim. Acta* **2017**, *255*, 391−395.
(31) Tan, T. L.; Wang, L. L.; Johnson, D. D.; Bai, K. Hydrogen Deposition on Pt(111) during Electrochemical Hydrogen Evolution from a First-Principles Multiadsorption-Site Study. *J. Phys. Chem. C* **2013**, *117*, 22696−22704.
(32) Magnussen, O. M.; Groß, A. Toward an Atomic-Scale Understanding of Electrochemical Interface Structure and Dynamics. *J. Am. Chem. Soc.* **2019**, *141*, 4777.
(33) Van den Bossche, M.; Skulason, E.; Rose-Petruck, C.; Jónsson, H. Assessment of Constant-Potential Implicit Solvation Calculations of Electrochemical Energy Barriers for H_2 Evolution on Pt. *J. Phys. Chem. C* **2019**, *123*, 4116−4124.
(34) Skúlason, E.; Tripkovic, V.; Björketun, M. E.; Gudmundsdóttir, S.; Karlberg, G.; Rossmeisl, J.; Bligaard, T.; Jónsson, H.; Nørskov, J. K. Modeling the Electrochemical Hydrogen Oxidation and Evolution Reactions on the Basis of Density Functional Theory Calculations. *J. Phys. Chem. C* **2010**, *114* (42), 18182−18197.
(35) Sundararaman, R.; Goddard, W. A., III; Arias, T. A. Grand canonical electronic density-functional theory: Algorithms and applications to electrochemistry. *J. Chem. Phys.* **2017**, *146* (11), 114104.
(36) Melander, M. M.; Kuisma, M. J.; Christensen, T. E. K.; Honkala, K. Grand-canonical approach to density functional theory of electrocatalytic systems: Thermodynamics of solid-liquid interfaces at constant ion and electrode potentials. *J. Chem. Phys.* **2019**, *150* (4), 041706.
(37) Lindgren, P.; Kastlunger, G.; Peterson, A. A. A Challenge to the G ∼ 0 Interpretation of Hydrogen Evolution. *ACS Catal.* **2020**, *10* (1), 121−128.
(38) Michaelides, A.; Hu, P. Catalytic Water Formation on Platinum: A First-Principles Study. *J. Am. Chem. Soc.* **2001**, *123*, 4235.
(39) Ishikawa, Y.; Mateo, J. J.; Tryk, D. A.; Cabrera, C. R. Direct Molecular Dynamics and Density-Functional Theoretical Study of the Electrochemical Hydrogen Oxidation Reaction and Underpotential Deposition of H on Pt(1 1 1). *J. Electroanal. Chem.* **2007**, *607* (1−2), 37−46.
(40) Hyman, M. P.; Medlin, J. W. Mechanistic Study of the Electrochemical Oxygen Reduction Reaction on Pt(111) Using Density Functional Theory. *J. Phys. Chem. B* **2006**, *110*, 15338−15344.
(41) Janik, M. J.; Taylor, C. D.; Neurock, M. First-Principles Analysis of the Initial Electroreduction Steps of Oxygen over Pt(111). *J. Electrochem. Soc.* **2009**, *156*, B126−B135.
(42) Sheng, T.; Lin, W.-F.; Hardacre, C.; Hu, P. Role of Water and Adsorbed Hydroxyls on Ethanol Electrochemistry on Pd: New Mechanism, Active Centers, and Energetics for Direct Ethanol Fuel Cell Running in Alkaline Medium. *J. Phys. Chem. C* **2014**, *118*, 5762−5772.
(43) Sakong, S.; Naderian, M.; Mathew, K.; Hennig, R. G.; Grob, A. Density Functional Theory Study of the Electrochemical Interface between a Pt Electrode and an Aqueous Electrolyte Using an Implicit Solvent Method. *J. Chem. Phys.* **2015**, *142* (23), 234107.
(44) Cheng, T.; Xiao, H.; Goddard, W. A., III Full atomistic reaction mechanism with kinetics for CO reduction on Cu(100) from ab initio molecular dynamics free-energy calculations at 298 K. *Proc. Natl. Acad. Sci. U. S. A.* **2017**, *114*, 1795−1800.
(45) Bunting, R. J.; Rice, P. S.; Thompson, J.; Hu, P. Investigating the Innate Selectivity Issues of Methane to Methanol: Consideration of an Aqueous Environment. *Chem. Sci.* **2021**, *12* (12), 4443−4449.
(46) Ouyang, Y.; Zhang, Y.; Rice, P. S.; Shi, L.; Wang, J.; Hu, P. Electrochemical CO2 reduction: Water/Catalyst Interface: Versus Polymer/Catalyst Interface. *J. Mater. Chem. A* **2021**, *9* (32), 17474−17480.
(47) Kronberg, R.; Laasonen, K. Coupling Surface Coverage and Electrostatic Effects on the Interfacial Adlayer-Water Structure of Hydrogenated Single-Crystal Platinum Electrodes. *J. Phys. Chem. C* **2020**, *124* (25), 13706−13714.
(48) Kronberg, R.; Laasonen, K. Reconciling the Experimental and Computational Hydrogen Evolution Activities of Pt(111) through DFT-Based Constrained MD Simulations. *ACS Catal.* **2021**, *11*, 8062−8078.
(49) Sumpter, B. G.; Getino, C.; Noid, D. W. Theory and application of neural computing in chemical science. *Annu. Rev. Phys. Chem.* **1994**, *45*, 439−481.
(50) Klanner, C.; Farrusseng, D.; Baumes, L.; Lengliz, M.; Mirodatos, C.; Schüth, F. The Development of Descriptors for Solids: Teaching "Catalytic Intuition" to a Computer. *Angew. Chem., Int. Ed.* **2004**, *43* (40), 5347−5349.
(51) Xu, J.; Cao, X.-M.; Hu, P. Accelerating Metadynamics-Based Free-Energy Calculations with Adaptive Machine Learning Potentials. *J. Chem. Theory Comput.* **2021**, *17* (7), 4465−4476.
(52) Behler, J. Constructing High-Dimensional Neural Network Potentials: A Tutorial Review. *Int. J. Quantum Chem.* **2015**, *115*, 1032−1050.
(53) Brown, D. F. R.; Gibbs, M. N.; Clary, D. C. Combining Ab Initio Computations, Neural Networks, and Diffusion Monte Carlo: An Efficient Method to Treat Weakly Bound Molecules. *J. Chem. Phys.* **1996**, *105* (17), 7597−7604.
(54) Kolb, B.; Luo, X.; Zhou, X.; Jiang, B.; Guo, H. High-Dimensional Atomistic Neural Network Potentials for Molecule-Surface Interactions: HCl Scattering from Au(111). *J. Phys. Chem. Lett.* **2017**, *8* (3), 666−672.
(55) Zhang, Y.; Zhou, X.; Jiang, B. Bridging the Gap between Direct Dynamics and Globally Accurate Reactive Potential Energy Surfaces Using Neural Networks. *J. Phys. Chem. Lett.* **2019**, *10*, 1185−1191.
(56) Li, J.; Song, K.; Behler, J. A Critical Comparison of Neural Network Potentials for Molecular Reaction Dynamics with Exact Permutation Symmetry. *Phys. Chem. Chem. Phys.* **2019**, *21* (19), 9672−9682.
(57) Quaranta, V.; Hellström, M.; Behler, J. Proton-Transfer Mechanisms at the Water-ZnO Interface: The Role of Presolvation. *J. Phys. Chem. Lett.* **2017**, *8* (7), 1476−1483.
(58) Huang, S.-D.; Shang, C.; Zhang, X. J.; Liu, Z. P. Material Discovery by Combining Stochastic Surface Walking Global Optimization with a Neural Network. *Chem. Sci.* **2017**, *8* (9), 6327−6337.
(59) Schlexer Lamoureux, P.; Winther, K.; Garrido Torres, J. A.; Streibel, V.; Zhao, M.; Bajdich, M.; Abild-Pedersen, F.; Bligaard, T. Machine Learning for Computational Heterogeneous Catalysis. *ChemCatChem* **2019**, *11*, 3581.
(60) Behler, J.; Martonak, R.; Donadio, D.; Parrinello, M. Metadynamics Simulations of the High-Pressure Phases of Silicon Employing a High-Dimensional Neural Network Potential. *Phys. Rev. Lett.* **2008**, *100*, 185501.
(61) Behler, J. Machine learning potentials for atomistic simulation. *J. Chem. Phys.* **2016**, *145*, 170901.
(62) Curtarolo, S.; Morgan, D.; Persson, K.; Rodgers, J.; Ceder, G. Predicting Crystal Structures with Data Mining of Quantum Calculations. *Phys. Rev. Lett.* **2003**, *91* (13), 135503−135504.
(63) Chmiela, S.; Sauceda, H. E.; Müller, K. R.; Tkatchenko, A. Towards Exact Molecular Dynamics Simulations with Machine-Learned Force Fields. *Nat. Commun.* **2018**, *9* (1), 3887.
(64) Huang, S. Da; Shang, C.; Kang, P. L.; Zhang, X. J.; Liu, Z. P. LASP: Fast Global Potential Energy Surface Exploration. *Wiley Interdiscip. Rev.: Comput. Mol. Sci.* **2019**, e1415.
(65) Shang, C.; Liu, Z.-P. Stochastic Surface Walking Method for Structure Prediction and Pathway Searchig. *J. Chem. Theory Comput.* **2013**, *9*, 1838−1845.
(66) Ma, S.; Shang, C.; Liu, Z. P. Heterogeneous Catalysis from Structure to Activity via SSW-NN Method. *J. Chem. Phys.* **2019**, *151* (5), 050901.
(67) Behler, J.; Parrinello, M. Generalized Neural-Network Representation of High-Dimensional Potential-Energy Surfaces. *Phys. Rev. Lett.* **2007**, *98* (14), 146401.

https://doi.org/10.1021/acs.jpclett.1c02998
J. Phys. Chem. Lett. 2021, 12, 10637−10645

(68) Huang, S.-D.; Shang, C.; Kang, P.-L.; Liu, Z.-P. Atomic Structure of Boron Resolved Using Machine Learning and Global Sampling. *Chem. Sci.* **2018**, *9*, 8644−8655.
(69) Grimme, S.; Antony, J.; Ehrlich, S.; Krieg, H. A Consistent and Accurate Ab Initio Parametrization of Density Functional Dispersion Correction (DFT-D) for the 94 Elements H-Pu. *J. Chem. Phys.* **2010**, *132* (15), 154104.
(70) Nilsson, A.; Pettersson, L. G. M. Perspective on the Structure of Liquid Water. *Chem. Phys.* **2011**, *389* (1−3), 1−34.
(71) Miceli, G.; De Gironcoli, S.; Pasquarello, A. Isobaric First-Principles Molecular Dynamics of Liquid Water with Nonlocal van Der Waals Interactions. *J. Chem. Phys.* **2015**, *142* (3), 034501.
(72) Gowers, R. J.; Carbone, P. A Multiscale Approach to Model Hydrogen Bonding: The Case of Polyamide. *J. Chem. Phys.* **2015**, *142* (22), 224907.
(73) Klimeš, J.; Bowler, D. R.; Michaelides, A. Van der Waals density functionals applied to solids. *Phys. Rev. B: Condens. Matter Mater. Phys.* **2011**, *83*, 195131.
(74) Le, J. B.; Fan, Q. Y.; Li, J. Q.; Cheng, J. Molecular Origin of Negative Component of Helmholtz Capacitance at Electrified Pt(111)/Water Interface. *Sci. Adv.* **2020**, *6* (41), No. eabb1219.
(75) Surendralal, S.; Todorova, M.; Neugebauer, J. Impact of Water Coadsorption on the Electrode Potential of H-Pt(1 1 1)-Liquid Water Interfaces. *Phys. Rev. Lett.* **2021**, *126* (16), 166802.
(76) Fomin, E.; Tatarkhanov, M.; Mitsui, T.; Rose, M.; Ogletree, D. F.; Salmeron, M. Vibrationally Assisted Diffusion of H2O and D2O on Pd(1 1 1). *Surf. Sci.* **2006**, *600* (3), 542−546.
(77) Limmer, D. T.; Willard, A. P.; Madden, P. A.; Chandler, D. Water exchange at a hydrated platinum electrode is rare and collective. *J. Phys. Chem. C* **2015**, *119*, 24016−24024.
(78) Wilke, S.; Natoli, V.; Cohen, M. H. Theoretical Investigation of Water Formation on Rh and Pt Surfaces. *J. Chem. Phys.* **2000**, *112* (22), 9986.
(79) Koper, M. T. M. Electrocatalysis: Theory and Experiment at the Interface. *Faraday Discuss.* **2009**, *140*, 11.
(80) Willard, A. P.; Limmer, D. T.; Madden, P. A.; Chandler, D. Characterizing Heterogeneous Dynamics at Hydrated Electrode Surfaces. *J. Chem. Phys.* **2013**, *138* (18), 184702.
(81) Rice, P. S.; Mao, Y.; Guo, C.; Hu, P. Interconversion of Hydrated Protons at the Interface between Liquid Water and Platinum. *Phys. Chem. Chem. Phys.* **2019**, *21* (11), 5932−5940.
(82) Sakong, S.; Groß, A. The Electric Double Layer at Metal-Water Interfaces Revisited Based on a Charge Polarization Scheme. *J. Chem. Phys.* **2018**, *149* (8), 084705.
(83) Pohl, M. N.; Muchová, E.; Seidel, R.; Ali, H.; Sršeň, Š.; Wilkinson, I.; Winter, B.; Slavíček, P. Do Water's Electrons Care about Electrolytes? *Chem. Sci.* **2019**, *10* (3), 848−865.
(84) Chandra, A. Effects of Ion Atmosphere on Hydrogen-Bond Dynamics in Aqueous Electrolyte Solutions. *Phys. Rev. Lett.* **2000**, *85* (4), 768.
(85) Zhang, X.-J. J.; Liu, Z.-P. P. Reaction Sampling and Reactivity Prediction Using the Stochastic Surface Walking Method. *Phys. Chem. Chem. Phys.* **2015**, *17* (4), 2757−2769.
(86) Zhang, X.-J. J.; Liu, Z.-P. P. Reaction Sampling and Reactivity Prediction Using the Stochastic Surface Walking Method. *Phys. Chem. Chem. Phys.* **2015**, *17* (4), 2757−2769.
(87) Fang, Y. H.; Wei, G. F.; Liu, Z. P. Catalytic Role of Minority Species and Minority Sites for Electrochemical Hydrogen Evolution on Metals: Surface Charging, Coverage, and Tafel Kinetics. *J. Phys. Chem. C* **2013**, *117* (15), 7669−7680.
(88) Yang, G.; Akhade, S. A.; Chen, X.; Liu, Y.; Lee, M.-S.; Glezakou, V.-A.; Rousseau, R.; Lercher, J. A. The Nature of Hydrogen Adsorption on Platinum in the Aqueous Phase. *Angew. Chem.* **2019**, *131* (11), 3565−3570.

https://doi.org/10.1021/acs.jpclett.1c02998
J. Phys. Chem. Lett. 2021, 12, 10637−10645